Geophysical Research Letters

RESEARCH LETTER
10.1029/2023GL105139

Potential Predictability of the Spring Bloom in the Southern Ocean Sea Ice Zone

Benjamin Buchovecky[1], Graeme A. MacGilchrist[2,3], Mitchell Bushuk[4], F. Alexander Haumann[2,5,6], Thomas L. Frölicher[7,8], Natacha Le Grix[7,8], and John Dunne[4]

[1]Department of Geosciences, Princeton University, Princeton, NJ, USA, [2]Program in Atmospheric and Oceanic Sciences, Princeton University, Princeton, NJ, USA, [3]School of Earth and Environmental Sciences, University of St. Andrews, St. Andrews, UK, [4]NOAA/OAR Geophysical Fluid Dynamics Laboratory, Princeton, NJ, USA, [5]Alfred Wegener Institute Helmholtz Centre for Polar and Marine Research, Bremerhaven, Germany, [6]Ludwig-Maximilian-University Munich, Munich, Germany, [7]Climate and Environmental Physics, Physics Institute, University of Bern, Bern, Switzerland, [8]Oeschger Centre for Climate Change Research, University of Bern, Bern, Switzerland

Abstract Every austral spring when Antarctic sea ice melts, favorable growing conditions lead to an intense phytoplankton bloom, which supports much of the local marine ecosystem. Recent studies have found that Antarctic sea ice is predictable several years in advance, suggesting that the spring bloom might exhibit similar predictability. Using a suite of perfect model predictability experiments, we find that November net primary production (NPP) is potentially predictable 7 to 10 years in advance in many Southern Ocean regions. Sea ice extent predictability peaks in late winter, followed by absorbed shortwave radiation and NPP with a 2 to 3 months lag. This seasonal progression of predictability supports our hypothesis that sea ice and light limitation control the inherent predictability of the spring bloom. Our results suggest skillful interannual predictions of NPP may be achievable, with implications for managing fisheries and the marine ecosystem, and guiding conservation policy in the Southern Ocean.

Plain Language Summary In very much the same way as we do for the weather, we can make forecasts of many aspects of the earth system. For example, rather than trying to predict how much rain will fall next Tuesday, we can explore how much algal growth might take place in the oceans around Antarctica in several months time. Such predictions could be extremely useful for managing the fragile ecosystems of these regions, for example, informing fishing quotas in an upcoming season. However, just like for weather forecasts, there are upper limits for how far into the future we can expect to accurately make such predictions. It's this upper limit that we try to understand in this theoretical modeling study. We find that the upper limit is actually rather long (as much as 10 years!), and show that this is because of the close relationship between algal growth and sea ice (ice formed at the ocean surface) in this cold polar region. In turn, the extent of the sea ice can be predicted a long time in advance because there is a lot "memory" in this component of the earth system.

Key Points:

- Southern Ocean net primary production (NPP) is potentially predictable seven to 10 years in advance in a perfect model experiment
- The peak predictability of NPP in November lags the peak predictability of sea ice extent and net shortwave radiation by 2 to 3 months
- Seasonal progression of predictability suggests that sea ice and light limitation control the inherent predictability of the spring bloom

Supporting Information:

Supporting Information may be found in the online version of this article.

Correspondence to:

G. A. MacGilchrist,
graeme.macgilchrist@gmail.com

Citation:

Buchovecky, B., MacGilchrist, G. A., Bushuk, M., Haumann, F. A., Frölicher, T. L., Le Grix, N., & Dunne, J. (2023). Potential predictability of the spring bloom in the Southern Ocean sea ice zone. *Geophysical Research Letters*, *50*, e2023GL105139. https://doi.org/10.1029/2023GL105139

Received 28 JUN 2023
Accepted 26 SEP 2023

Author Contributions:

Conceptualization: Graeme A. MacGilchrist, Mitchell Bushuk, F. Alexander Haumann, Thomas L. Frölicher
Data curation: Thomas L. Frölicher, Natacha Le Grix
Formal analysis: Benjamin Buchovecky
Funding acquisition: Thomas L. Frölicher
Investigation: Benjamin Buchovecky, Graeme A. MacGilchrist, Mitchell Bushuk

1. Introduction

Marine ecosystems are sustained at their base by net primary production (NPP). Variations in NPP cascade upward to higher trophic levels, driving variations in living marine organisms (e.g., zooplankton, or krill), which are sensitive to changing environmental conditions (Chassot et al., 2010; Stock et al., 2014; Tagliabue et al., 2021). In the Southern Ocean's seasonal ice zone, where sea ice seasonally extends and retreats, phytoplankton grow intensely for a relatively short period (<10 weeks) during the austral spring, resulting in a rapid increase in NPP (Arrigo et al., 2008; Arteaga et al., 2020; Douglas et al., 2023; Moore & Abbott, 2000; Uchida et al., 2019). In the subpolar Southern Ocean, across both the seasonal ice zone and Antarctic coastal polynyas (a region that we collectively call the sea ice zone), the spring increase in NPP from intense phytoplankton growth accounts for as much as 15% of total annual NPP in the Southern Ocean (Arrigo et al., 2008; Taylor et al., 2013). These short annual periods of intense growth, or blooms, are thus an important driver of the Southern Ocean marine ecosystem. Even though the relationship between NPP and upper trophic level biomass is complex (Friedland et al., 2012; Stock et al., 2017), skillful predictions of monthly NPP on seasonal-to-interannual time scales that capture the fluctuations in spring bloom production may help to better constrain predictions of ecological quantities and assist stakeholders in fishery management and marine conservation (Brooks & Ainley, 2022; Deppeler & Davidson, 2017; Moreau et al., 2020).

Methodology: Graeme A. MacGilchrist, Mitchell Bushuk, F. Alexander Haumann, Thomas L. Frölicher, Natacha Le Grix, John Dunne
Project Administration: Graeme A. MacGilchrist, Mitchell Bushuk, Thomas L. Frölicher
Software: Benjamin Buchovecky, Graeme A. MacGilchrist, Thomas L. Frölicher
Supervision: Graeme A. MacGilchrist, Mitchell Bushuk, F. Alexander Haumann
Validation: Benjamin Buchovecky
Visualization: Benjamin Buchovecky, Graeme A. MacGilchrist, Mitchell Bushuk, F. Alexander Haumann
Writing – original draft: Benjamin Buchovecky
Writing – review & editing: Benjamin Buchovecky, Graeme A. MacGilchrist, Mitchell Bushuk, F. Alexander Haumann, Thomas L. Frölicher, Natacha Le Grix, John Dunne

The spring bloom is closely linked to the seasonal retreat of sea ice (Arrigo et al., 2008; Arteaga et al., 2020; Moore & Abbott, 2000; Uchida et al., 2019), which has been shown to be predictable. Perfect model (PM) experiments, which assess the "potential predictability" of the climate state assuming perfectly known initial conditions and perfectly known model physics, show that the Antarctic sea ice edge location has interannual predictability with lead times of up to 3 years (Holland et al., 2013; Marchi et al., 2019). Using suites of initialized hindcasts from a General Circulation Model (GCM), Bushuk et al. (2021) found that observed winter Antarctic sea ice extent (SIE) can be skillfully predicted with an 11-month lead in the Weddell, Amundsen/Bellingshausen, Indian, and West Pacific sectors. These PM experiments and GCM-based hindcasts attribute the predictability and prediction skill of Antarctic sea ice to the significant thermal inertia of the ocean which causes ocean heat content anomalies to remain at depth over the summer and reemerge during the autumnal sea ice advance, while being transported by the mean ocean circulation (Bushuk et al., 2021; Holland et al., 2013; Marchi et al., 2019).

Over the past decade, the potential for skillful seasonal-to-interannual predictions of marine primary production has been shown (Séférian et al., 2014; Park et al., 2019; Frölicher, Ramseyer, et al., 2020). This work has revealed that skill exists in locations where the rate of phytoplankton growth is determined by a process that itself exhibits predictability, for example, nutrient supply (Brune et al., 2022; Ham et al., 2021; Krumhardt et al., 2020). To date, no study has focused on the sea ice zone. Given the robust seasonal prediction skill of Antarctic SIE and the importance of sea ice to the sea ice zone spring bloom, we ask the question: How predictable is spring bloom NPP in the Southern Ocean sea ice zone and what are the main drivers of spring bloom predictability?

In this study, we assess the regional potential predictability of spring bloom NPP in the Southern Ocean using a suite of PM experiments performed with an Earth System Model (ESM). In this case, the PM framework determines the upper limit of predictability in the system assuming perfect representation of biogeochemical dynamics in addition to physics. After finding that spring bloom NPP and its associated physical drivers are predictable on seasonal-to-interannual time scales, we use a lead/lag diagnostic correlation analysis to elucidate the mechanisms of NPP predictability in this model.

2. Methodology

Model simulations were performed with the Earth System Model ESM2M (Dunne et al., 2012, 2013) developed by the Geophysical Fluid Dynamics Laboratory (GFDL). The GFDL-ESM2M model is a fully coupled ESM with atmosphere, land, ocean, and sea ice components, and includes interactive ocean biogeochemistry. The atmosphere component is nearly identical to that in the GFDL Climate Model 2.1 (Delworth et al., 2006) and has 24 vertical layers with a horizontal resolution of 2° latitude by 2.5° longitude. The ocean component uses the MOM4 model (Griffies et al., 2005) with 50 vertical layers and a nominal horizontal grid resolution of 1° latitude by 1° longitude, refined smoothly to 1/3° resolution at the equator. The sea ice component uses the same grid as the ocean component and simulates three thermodynamic layers, five ice thickness categories, and elastic-viscous-plastic sea ice dynamics (Winton, 1999).

The GFDL-ESM2M model simulates ocean biogeochemistry using the Tracers of Ocean Phytoplankton with Allometric Zooplankton version 2.0 (TOPAZv2), which models 30 tracers to describe cycles of carbon, nitrogen, phosphorus, silicon, iron, oxygen, alkalinity, lithogenic material, and surface sediment calcite (Dunne et al., 2013). TOPAZv2 resolves three phytoplankton groups: small (cyanobacteria and picoeukaryotes), large (diatoms and other eukaryotes), and diazotrophs (nitrogen-fixing phytoplankton). The rate of phytoplankton growth depends on irradiance, nutrient availability, and temperature. Organic biomass is lost through grazing by zooplankton and direct bacterial respiration. In this study, we consider NPP integrated over the top 100 m of the ocean, where the majority of phytoplankton growth takes place.

The fidelity of the simulation's representation of Southern Hemisphere sea ice has been presented in Dunne et al. (2012) and Frölicher, Aschwanden, et al. (2020) (see their Figures 10 and 11, respectively). The model has a low bias in sea-ice concentration and extent in the Weddell Gyre in particular (due to the emergence of large open ocean polynyas, discussed further in Text S2 in Supporting Information S1) but broadly captures the seasonal cycle. Representation of NPP is challenging to assess in this part of the ocean, considering the paucity of comprehensive observations. Comparison to satellite ocean color (Dunne et al., 2013, see their Figure 3) and observation-based estimates of NPP (Le Grix et al., 2022, see their Figure B1) shows that the model captures the right order of magnitude of biological activity close to the Antarctic continent, but generally has a positive bias in

open ocean regions such as the eastern Weddell Gyre. Figure S1 in Supporting Information S1 shows that NPP in a historically forced simulation of GFDL-ESM2M has low variance on inter-annual timescales in comparison to observation-based products, particularly in open-ocean regions (note that this figure is a deseasonalized version of Figure B1 from Le Grix et al., 2022). Again, shelf and coastal regions exhibit comparatively favorable fidelity. This figure also shows the wide spread in observational estimates in this region. The model represents surface and subsurface nutrients well, but overestimates subsurface oxygen (Dunne et al., 2013)—a bias that can likewise be traced to the intermittent emergence of open ocean polynyas.

We use a preindustrial control simulation and a suite of PM experiments conducted with GFDL-ESM2M as described in Frölicher, Ramseyer, et al. (2020). A 300-year preindustrial control simulation is branched from a 1000-year quasi-steady-state simulation initialized with conditions from 1860 (Dunne et al., 2012). The PM experiments branch off from the preindustrial control simulation at six different start dates: January 1st in the years 22, 64, 106, 170, 232, and 295 (years chosen at random). Each start date contains 40 ensemble members, each initialized with an infinitesimal perturbation in sea surface temperature (SST) added to a single grid cell in the Weddell Sea. The perturbations applied to the ensemble members were evenly distributed between 0.002 and −0.002°C. Each ensemble member was forced with identical preindustrial boundary conditions and was run for a duration of 10 years with the last ensemble group extending beyond the preindustrial control simulation by 5 years. The temporal resolution of all variables analyzed here is monthly mean.

We use the prognostic potential predictability (PPP) metric to assess the predictability of NPP and quantities relevant to the spring bloom. The PPP is an estimate of the inherent upper limit of prediction skill of a given model. From Pohlmann et al. (2004), PPP is given by the following equation:

$$PPP(\tau) = 1 - \frac{\frac{1}{N(M-1)} \sum_{j=1}^{N} \sum_{i=1}^{M} \left(X_{ij}(\tau) - \overline{X}_j(\tau) \right)^2}{\sigma_c^2}$$

where X_{ij} is the value of a given variable for the ith ensemble member of the jth ensemble, $\overline{X}_j$ is the jth ensemble mean, σ_c^2 is the variance of the control simulation for a given target month, N is the number of ensembles ($N = 6$), M is the number of ensemble members ($M = 40$), and τ is the forecast lead time. Intuitively, PPP assesses how ensemble members chaotically diverge over time by comparing the ensemble spread to the natural variability of the control simulation. When PPP is equal to zero, the ensemble spread is identical to the simulated natural variability of the control simulation, which indicates that the variable could not have been skillfully predicted from the initial conditions. When PPP is equal to one, the spread of the ensemble members is perfectly distinguishable from the simulated natural variability which indicates that the model is capable of perfectly predicting the variable given accurate initial conditions.

For our diagnostic analysis, we compute the Pearson correlation coefficient between NPP at a target month and a predictor variable at months leading the target month. We perform this correlation analysis for all 12 target months with a maximum lead time of 13 months. For both the PM predictability assessment and diagnostic correlation analysis, we consider six sectors of the Southern Ocean in our study: Weddell (60°W–20°E), Indian (20°E−90°E), West Pacific (90°E−160°E), Ross (160°E−130°W), and Amundsen and Bellingshausen (130°W–60°W), plus the pan-Antarctic region, which encompasses all aforementioned sectors, following Bushuk et al. (2021). To capture the sea ice zone, the northern boundary for all sectors is 55°S and the southern boundary is the Antarctic continent. The sector boundaries are shown in Figure S2 in Supporting Information S1, and seasonal climatologies of relevant variables in each sector are shown in Figure S3 in Supporting Information S1. We perform an F-test with the ensemble and control run variances to determine significant PPP values above the 95% confidence level (PPP > 0.183), and use a t-test that accounts for autocorrelation following Bretherton et al. (1999) to determine significant correlation coefficients above the 95% confidence level.

3. Results

Figure 1 shows PPP time series for NPP over the 10-year forecast period. Since the suite of PM experiments are initialized on January 1st, near perfect NPP potential predictability (PPP > 0.9) exists in January of the first year (Figure 1; see bottom-left corner of each panel). At longer forecast times, NPP potential predictability decreases as the initial perturbations of the ensemble members grow chaotically and diverge, making it more difficult to

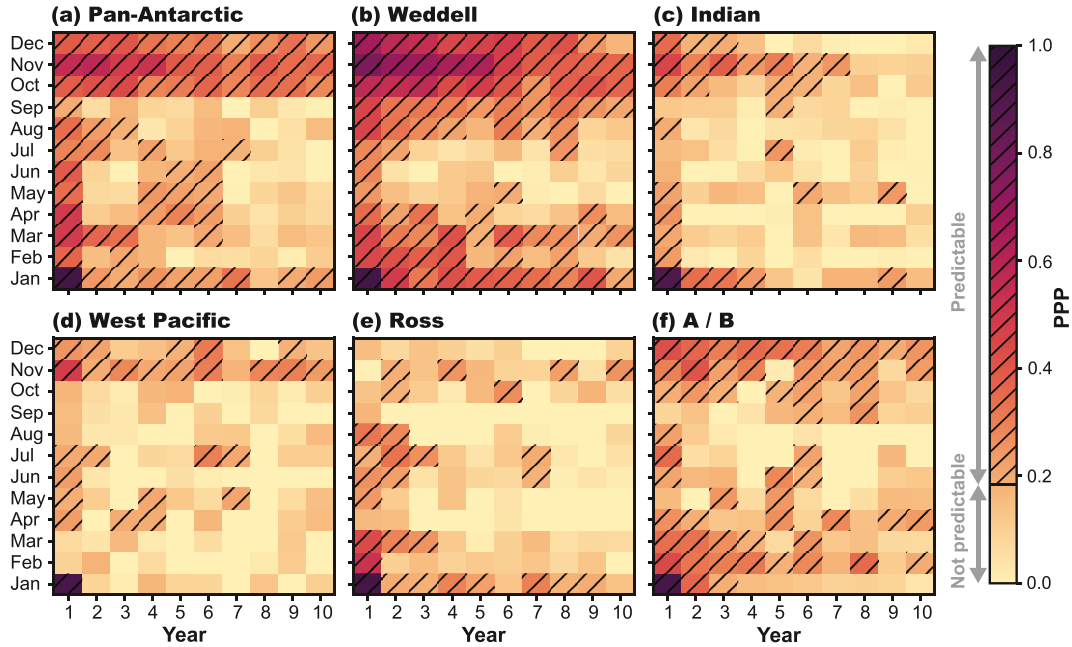

Figure 1. Regional predictability of net primary production given by the prognostic potential predictability (PPP) metric computed from a suite of perfect model (PM) experiments with the GFDL-ESM2M model. The full 10-year forecast period from the PM ensembles is displayed with forecast years on the *x*-axis and months on the *y*-axis. PPP values above the 0.183 significance threshold are hatched and have a 95% confidence level based on an *F*-test.

predict their future state from the initial conditions. Across all regions, the highest PPP values occur in spring, from October to December, indicating that spring NPP is potentially predictable. NPP in the Weddell sector (Figure 1b) has the highest spring PPP throughout the forecast period, maintaining predictability for NPP in September through December beyond the 10 years lead times. The Indian (Figure 1c) and West Pacific sectors (Figure 1d) have lower PPP than the Weddell sector, but PPP remains significant in November for several years. NPP in the Amundsen/Bellingshausen sector (Figure 1f) has high PPP for up to 10 years in the spring with maximum PPP in December. Unlike the other sectors, Ross sector NPP does not have consistently significant PPP in the spring (Figure 1e), though it is notable that significant values re-emerge a couple of months later, in January, after the climatological peak in NPP. While we show that NPP is predictable on interannual time scales, the highest PPP values (>0.4) occur in November of the first forecast year, suggesting that nearly half of the spring NPP variance can be predicted almost 1 year in advance. We focus our further analysis on this first-year November maximum to elucidate the key drivers of NPP predictability.

Figure 2 shows the regional predictability of NPP and potential key drivers of the sea ice zone spring bloom—sea ice extent (SIE), mixed-layer depth (MLD), surface irradiance (IRR_{SFC}), and surface dissolved iron (FED_{SFC})—for the first 13 months of the forecast period. As in Figure 1, NPP predictability peaks in November for the pan-Antarctic (Figure 2a), Weddell (Figure 2b), Indian (Figure 2c), and West Pacific (Figure 2d) sectors while the Amundsen/Bellingshausen (A/B; Figure 2f) sector has maximum NPP predictability in December. Spring NPP is generally unpredictable in the Ross sector (Figure 2e). In the Pan-Antarctic case, as well as prominently in the Weddell, Indian, West Pacific, and A/B, the November peak in NPP predictability is preceded by—at 1 to 2 month leads—that of SIE and IRR_{SFC}, indicating that the alleviation of light limitation could be a prominent source of NPP predictability. Peaks in SIE predictability are accompanied, or slightly preceded, by peaks in MLD predictability (in all except the West Pacific and Ross sectors). This correspondence likely stems from the close link between SIE predictability and the characteristics of the mixed layer, which mediate the upward mixing of subsurface heat (Bushuk et al., 2021; Libera et al., 2022). In the A/B and, to a lesser extent, Indian sectors, the timing of high surface iron predictability—which follows that of the MLD and precedes that of NPP—indicates that alleviation of nutrient limitation could be an important source of NPP predictability in that area. While wintertime iron predictability is high in other areas (specifically the Weddell and Ross sectors), its alignment with spring bloom NPP predictability is less clear. In the following, we highlight the potential role played by SIE

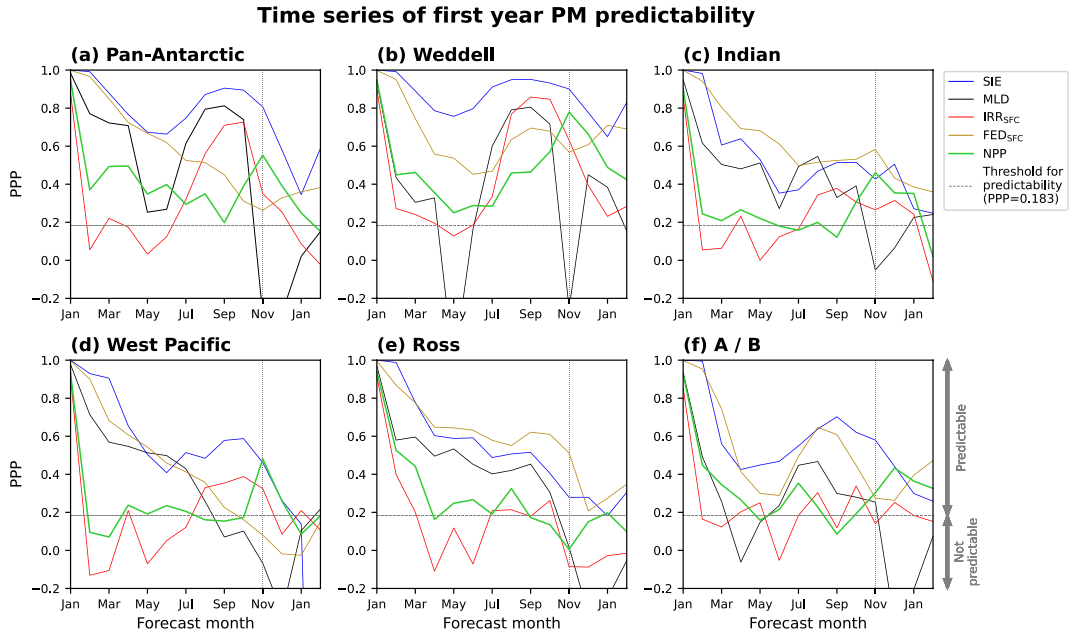

Figure 2. Regional predictability of sea ice extent (SIE), mixed layer depth (MLD), surface irradiance (IRR$_{SFC}$), surface dissolved iron (FED$_{SFC}$), and net primary production (NPP) determined by the prognostic potential predictability (PPP) metric. The dotted vertical line marks November in the first forecast year. PPP values above 0.183 (horizontal dashed line) are significant at a 95% confidence level based on an *F*-test. PPP values above the significance threshold indicate that anomalies of the given variable are predictable with the ESM2M model given perfect initial conditions.

and IRR$_{SFC}$ as a source of NPP predictability, and revisit the role of iron in the discussion. Although temperature impacts NPP, it plays a mediating rather than limiting role and, as a result, its impact on predictability is secondary (see Text S1 in Supporting Information S1).

In Figure 3, we arrange key spring bloom drivers and NPP according to the timing of their respective peaks in predictability. We also add the PM predictability of surface chlorophyll *a* (CHL) concentration and surface biomass (BIOM) since these metrics can be estimated using satellite (Behrenfeld et al., 2017) and biogeochemical float (Arteaga et al., 2020) data, and could be integrated into operational forecasts informed by these PM predictability results. Aside from the Ross sector, all regions exhibit a diagonal structure in their predictability peaks in Figure 3, suggesting a progression of predictability starting with SIE and MLD, followed by IRR$_{SFC}$, and finally NPP. The pan-Antarctic (Figure 3a), Weddell (Figure 3b), and Indian (Figure 3c) sectors have the most defined progression of predictability with a 2 to 3 months lag between maximum SIE and NPP predictability. In these regions, we also see maximum predictability for chlorophyll *a* and surface biomass lagging the November peak in NPP predictability by 1 to 3 months. The West Pacific (Figure 3d) and Amundsen/Bellingshausen (Figure 3f) sectors display a less defined diagonal structure but still exhibit a 2 to 3 months lag between maximum SIE and NPP predictability. An equivalent perspective for the progression of predictability from MLD, to surface iron, to NPP (Figure S6 in Supporting Information S1) shows that while it may be present in some sectors (specifically A/B, Weddell, and Indian), it is notably absent in others, and for the Pan-Antarctic. In either case, these results support the interpretation that the spring bloom mechanism (Figure 3g, further discussed below) causes the elevated predictability of spring NPP in the model simulations.

To further examine the spring bloom and the relationship between its drivers and NPP, we perform a correlation analysis of SIE and IRR$_{SFC}$ anomalies preceding NPP anomalies up to 13 months in advance using the 300-year preindustrial control simulation (Figure 4). The colormap reveals the correlation of NPP in each target month (displayed along the *x*-axis) with SIE (top) and IRR$_{SFC}$ (bottom; positive downwards) for each lead time (displayed along the *y*-axis). For example, the value at target month November and lead 3 months provides the correlation between November NPP and SIE/IRR$_{SFC}$ in the previous August. Outside of September to March, values of NPP are vanishingly small in both magnitude and variance (because it is polar night). Consequently, correlations during these months could be spurious and rather meaningless. In line with this, the regression

10.1029/2023GL105139

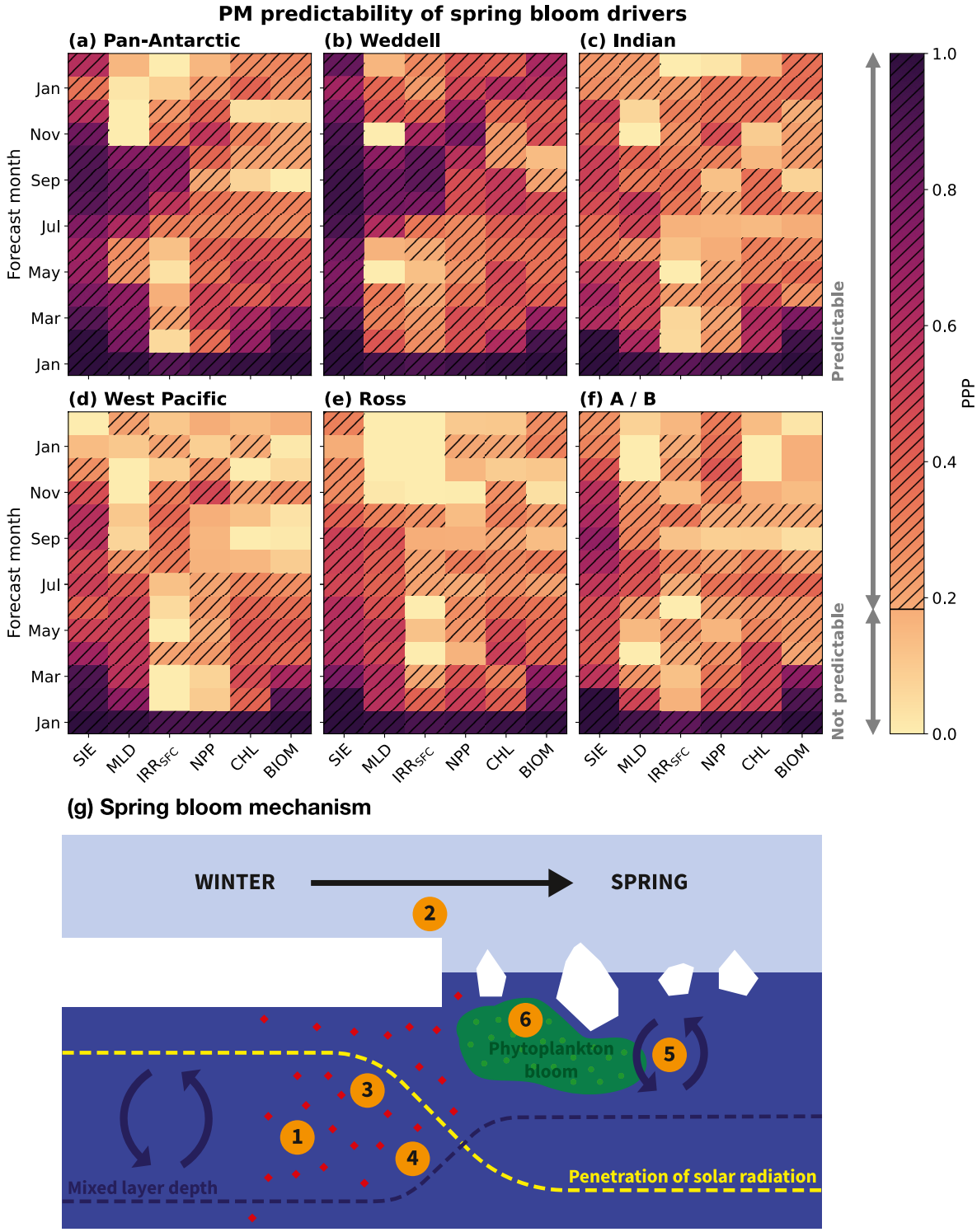

Figure 3. (a–f) Regional predictability of sea ice extent (SIE), mixed layer depth (MLD), surface irradiance (IRR_{SFC}), net primary production (NPP), Chl *a* (CHL), and surface biomass (BIOM) given by the prognostic potential predictability metric computed from a suite of Perfect model experiments. Here, we display the first year of forecast time and arrange the variables on the *x*-axis following what we expect from the climatological spring bloom mechanism. (g) The mechanism of the climatological spring phytoplankton bloom. 1) Accumulation of nutrients in mixed layer during winter. 2) Sea ice melts and retreats. 3) Ocean surface receives more solar radiation, penetrates deeper into the water column. 4) The MLD shoals due to an influx of fresh melt water and greater solar radiation. 5) The shallow MLD traps phytoplankton and nutrients near the surface where light is abundant. 6) Phytoplankton grows intensely in the favorable conditions, forming the spring bloom.

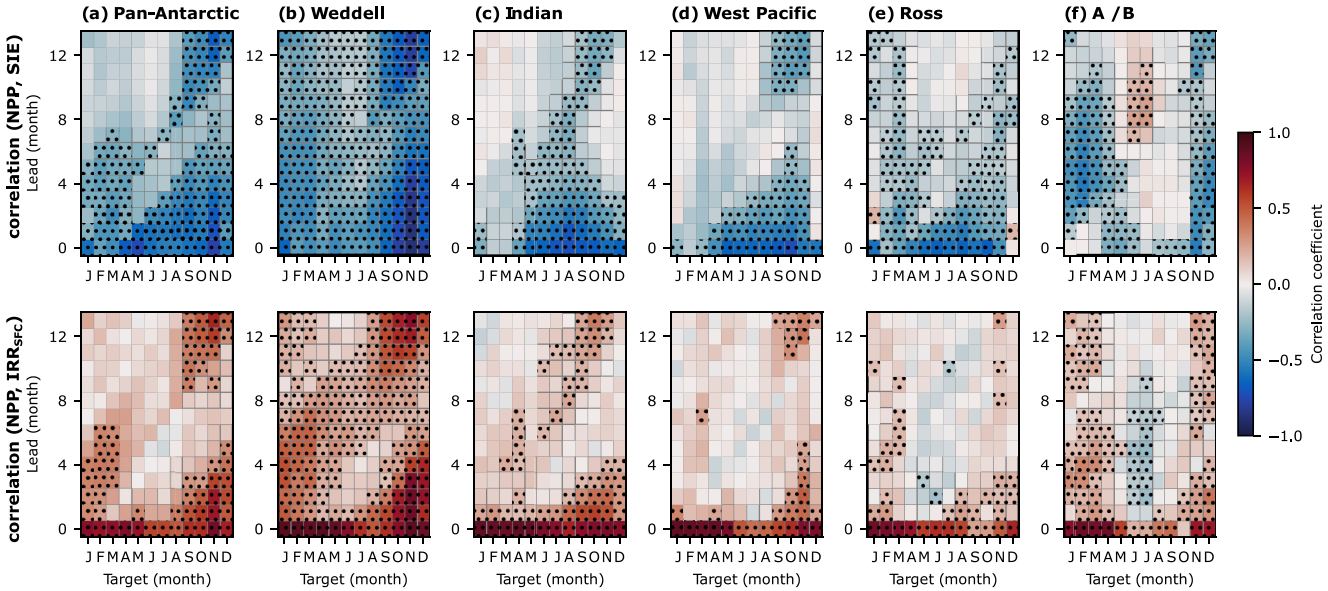

Figure 4. In the upper row, the Pearson correlation coefficient of net primary production (NPP) anomalies at target months January through December and sea ice extent anomalies at 0–13 lead months in the (a) pan-Antarctic, (b) Weddell, (c) Indian, (d) West Pacific, (e) Ross, and (f) Amundsen/Bellingshausen sectors. In the lower row, the Pearson correlation coefficient of NPP anomalies at the same target months and surface irradiance (IRR_{SFC}) anomalies at the same lead months. Correlation values are computed from the 300-year preindustrial control simulation. The dotting indicates Pearson correlation coefficient values significant at the 95% confidence level according to a *t*-test accounting for autocorrelation.

coefficient (not shown) is substantially smaller in these months than during the spring and summer. Consistent with our proposed spring bloom predictability mechanism (Figure 3g), we find a strong inverse relationship between NPP and SIE in all sectors, which means anomalously low SIE leads to anomalously high NPP, and vice versa. The relationship is strongest in the Weddell sector (Figure 4a) where November NPP anomalies have high correlation ($r < -0.75$) with SIE anomalies up to five lead months. The correlation is lower in the other sectors, but these sectors also exhibit statistically significant negative correlation of November NPP anomalies with earlier SIE anomalies up to five lead months. In all sectors aside from the Ross Sea, we also find significant correlation between November NPP anomalies and SIE anomalies from the previous year, corresponding to a winter-to-winter reemergence of SIE anomalies. When examining IRR_{SFC} as a predictor of NPP, we find a strong positive relationship in all sectors, consistent with the expectation that increased light availability drives enhanced NPP. The positive IRR_{SFC} correlations with November NPP anomalies are significant at shorter lead times than the SIE correlations anomalies, but significant correlation is maintained up to 4 months lead, as well as lead time beyond 1 year in all regions except for the Ross Sea. This analysis suggests that if late winter and early spring SIE and IRR_{SFC} can be skillfully predicted, they should provide associated predictability for spring NPP, supporting the proposed predictability mechanism shown in Figure 3. The same correlation analysis was carried out for surface iron (Figure S7 in Supporting Information S1). Spring and summertime NPP is positively correlated with the previous winter's surface iron concentrations in most sectors, but with correlation coefficients somewhat lower than that of IRR_{SFC} and SIE, particularly for a target month of November, the month of maximum NPP predictability.

4. Discussion and Conclusions

Given the significant influence of NPP variations on marine ecosystems and emerging capabilities in biogeochemical modeling and data assimilation, there have been multiple recent studies assessing the predictability of NPP using ESMs on interannual time scales (e.g., Brune et al., 2022; Chikamoto et al., 2015; Frölicher, Ramseyer, et al., 2020; Krumhardt et al., 2020; Park et al., 2019; Séférian et al., 2014; Taboada et al., 2019). However, the Southern Ocean seasonal ice zone, which differs from other regions due to the seasonal advance and retreat of sea ice and associated drastic changes in the environmental conditions, has received little attention so far. Here, we use a suite of PM experiments performed with the GFDL-ESM2M model to assess the predictability of NPP and then examine how variations in sea ice retreat influence the predictability of NPP. We find that NPP

is predictable 7 to 10 years in advance in all regions except the Ross sector (Figure 1). NPP predictability tends to peak in November (11 months from the January first initialization date), suggesting that skillful predictions of NPP on seasonal to interannual time scales could be possible given accurate initial conditions. Moreover, since SIE provides the dominant source of spring NPP predictability and recent studies have shown skillful operational seasonal predictions of Antarctic SIE (e.g., Bushuk et al., 2021; Morioka et al., 2019), skillful NPP predictions may be practically within reach.

In a Pan-Antarctic sense, and across most sectors, the progression of predictability from SIE and MLD, to IRR_{SFC}, and to NPP with a 2 to 3 months lag (Figures 2 and 3a–3f) supports our hypothesis that the spring bloom mechanism—relating the seasonal growth and melt of sea ice to both nutrient and light availability (Figure 3g)—exerts control over the inherent predictability time scales of NPP and other spring bloom quantities. The correlation analysis (Figure 4) shows a strong relationship between springtime NPP anomalies and earlier SIE and IRR_{SFC} anomalies, supporting the PM predictability results. The sequence of these relationships aligns with what we causally expect given the spring bloom mechanism. Negative correlation between NPP and earlier SIE is expected since greater SIE inhibits phytoplankton growth by limiting light. Positive correlation between IRR_{SFC} and NPP also agrees with the spring bloom mechanism since greater surface irradiance increases light availability, which promotes phytoplankton growth.

Nutrient availability could also play an important role in the predictability of NPP in some regions. The PM and correlation analyses (Figure 2, and Figures S6 and S7 in Supporting Information S1) indicate that predictability of wintertime nutrient concentrations are important for springtime NPP predictability in the A/B sector, and could play a role in the Weddell and Indian sectors. As prior work has indicated (Krumhardt et al., 2020), the major source of predictability is likely to come from whichever factor (light or nutrients) is most commonly limiting growth during the month of the spring bloom. While the model diagnostics necessary to assess this comprehensively were not archived for these experiments, the model's climatological seasonal cycle indicates that surface iron concentrations are not exhausted until January or February, supporting the possibility that November-time growth is not iron limited (Figure S3 in Supporting Information S1). Further work, including assessing nutrient and light limitation within a PM framework, is required to fully assess the relative impact of these drivers on NPP. The balance of these mechanisms has significant ramifications for the translation of "potential predictability" into real world prediction skill, since observational constraints for sea-ice extent and MLD are notably more abundant than those for nutrients.

There are clear regional differences in the predictability of NPP and other spring bloom quantities. The Weddell sector is consistently more predictable than all other regions, while the Ross sector is consistently the least predictable. The low predictability of NPP in the Ross sector is accompanied by low predictability in sea-ice (Figure 2). The anomalously low sea ice predictability of the Ross Sea has also been identified in earlier work on seasonal predictions with other GFDL models (Bushuk et al., 2021), PM experiments performed with CCSM3 (Holland et al., 2013), and multi-model predictions submitted to SIPN-South (Massonnet et al., 2020). Bushuk et al. (2021) speculated that the low Ross Sea ice predictability could be related to the strong meridional ice drift in this region, which implies that sea ice dynamics have a larger influence on the Ross sea ice edge position compared to other Antarctic regions. Since these ice dynamics are largely driven by unpredictable winds, this potentially makes the sea ice edge more difficult to predict in this region. The spring bloom mechanism described above suggests that the inherent challenges in predicting Ross sea ice may translate to inherently low predictability of Ross NPP. However, the robustness of low Ross Sea predictability is still quite uncertain, as the multi-model PM study of Marchi et al. (2019) shows that there is substantial model diversity in Ross sea ice predictability, with some models exhibiting high predictability in this region.

It is important to note that the real-world applicability of the timescales and mechanisms of predictability found in this study depends inherently on the fidelity of the model's representation of primary production in the Southern Ocean sea ice zone. In Section 2 we noted that the GFDL-ESM2M model captures large-scale biogeochemical processes reasonably well (Dunne et al., 2012, 2013; Frölicher, Aschwanden, et al., 2020; Le Grix et al., 2022), but exhibits a notably low bias in interannual variability of NPP in the sea-ice zone (Figure S1 in Supporting Information S1). It is likely that certain processes, such as the dynamic link between NPP and sea-ice cover (a key component of the predictability in the model), are more complex in reality. For example, although the model allows under-ice production, there is no representation of ice-associated algae, and it is questionable to what extent it is able to accurately capture the exact timing of the phytoplankton bloom in the Southern Ocean.

Recent observations suggest that biomass starts increasing under sea ice prior to its retreat (Horvat et al., 2022), though peak biomass accumulation is expected in November (Arteaga et al., 2020; Llort et al., 2015), which is consistent with the month of peak predictability in our experiments. Additionally, the biogeochemical model in ESM2M (TOPAZv2) lacks an explicit representation of zooplankton (Dunne et al., 2013), with phytoplankton loss via grazing represented as a function of phytoplankton abundance and temperature. Consequently, top-down controls, which could play an important role in the evolution of the spring bloom in the Southern Ocean (Rohr et al., 2017), are not fully represented. Finally, like many global models, GFDL-ESM2M exhibits multi-decadal variability in the subpolar Southern Ocean, and this is a source of bias in several aspects of the model's physical and biogeochemical state. In Text S2 in Supporting Information S1, we show that our results are not sensitive to the timing of initialization with respect to the phase of this variability. Broadly, this study should be taken as an estimate of the timescales and mechanisms of potential predictability, while acknowledging that the model may not capture some of the nuances of bloom dynamics in the sea ice zone.

In summary, we have assessed the potential predictability of NPP in the GFDL-ESM2M model using a suite of PM experiments. Given the important role of sea ice retreat in the spring bloom mechanism and recent work indicating that sea ice is predictable on seasonal-to-interannual time scales, we hypothesized that NPP and quantities relevant to the spring bloom should be predictable on similar time scales. Supporting our hypothesis, we find that November NPP is potentially predictable in all regions except the Ross sector for 7 to 10 years in advance, with highest potential predictability in the Weddell sector. By examining the timing of the peak in predictability across quantities relevant to the spring bloom, we find a temporal progression of maximum potential predictability from SIE and MLD, to IRR_{SFC}, and to NPP with a 2 to 3 months lag, aligning with the climatological spring bloom mechanism. Lead-time correlations of SIE predicting NPP and IRR_{SFC} predicting NPP further support the progression of predictability. While the robustness of these results still must be corroborated with other ESMs, the existence of NPP potential predictability and the progression of predictability from SIE suggests that if we can initialize a model accurately and skillfully predict SIE, then prediction skill should exist for November NPP, potentially extending years in advance. Such skillful NPP predictions would be critical for predicting ecosystem changes and the biomass of living marine organisms, guiding fishery management, and informing marine conservation.

Data Availability Statement

Data and Jupyter notebooks to reproduce the figures in this manuscript are available on Zenodo (Buchovecky et al., 2023).

Acknowledgments

This work was supported by the High Meadows Environmental Institute at Princeton University and the NSF's Southern Ocean Carbon and Climate Observations and Modeling (SOCCOM) Project under the NSF Award PLR-1425989. F.A.H. was supported by NASA Grant 80NSSC19K1115 and by the European Union (ERC, VERTEXSO, 101041743). G.A.M was supported under SOCCOM and UKRI Grant MR/W013835/1. T.L.F was supported by Swiss National Science Foundation (Grant P00P2_198897) and the Swiss National Supercomputing Centre. N.L was supported by the European Union's Horizon 2020 research and innovation program under Grant 820989 (project COMFORT) and no. 862923 (project AtlantECO) as well as the Bretscher Funds. We are grateful to Yushi Morioka, Jessica Luo, and two anonymous reviewers for insightful comments on the manuscript, and Keith Rodgers for help in setting up the model experiments.

References

Arrigo, K. R., van Dijken, G. L., & Bushinsky, S. (2008). Primary production in the southern ocean, 1997–2006. *Journal of Geophysical Research*, *113*(C8), C08004. https://doi.org/10.1029/2007JC004551

Arteaga, L. A., Boss, E., Behrenfeld, M. J., Westberry, T. K., & Sarmiento, J. L. (2020). Seasonal modulation of phytoplankton biomass in the southern ocean. *Nature Communications*, *11*(1), 5364. https://doi.org/10.1038/s41467-020-19157-2

Behrenfeld, M. J., Hu, Y., O'Malley, R. T., Boss, E. S., Hostetler, C. A., Siegel, D. A., et al. (2017). Annual boom–bust cycles of polar phytoplankton biomass revealed by space-based lidar. *Nature Geoscience*, *10*(2), 118–122. https://doi.org/10.1038/ngeo2861

Bretherton, C. S., Widmann, M., Dymnikov, V. P., Wallace, J. M., & Bladé, I. (1999). The effective number of spatial degrees of freedom of a time-varying field. *Journal of Climate*, *12*(7), 1990–2009. https://doi.org/10.1175/1520-0442(1999)012⟨1990:TENOSD⟩2.0.CO;2

Brooks, C. M., & Ainley, D. G. (2022). A summary of United States research and monitoring in support of the Ross sea region marine protected area. *Diversity*, *14*(6), 447. https://doi.org/10.3390/d14060447

Brune, S., Espejo, M. E. C., Nielsen, D. M., Li, H., Ilyina, T., & Baehr, J. (2022). Oceanic Rossby waves drive inter-annual predictability of net primary production in the central tropical Pacific. *Environmental Research Letters*, *17*(1), 014030. https://doi.org/10.1088/1748-9326/ac43e1

Buchovecky, B., MacGilchrist, G., Bushuk, M., Haumann, A., Frölicher, T., Le Grix, N., & Dunne, J. (2023). Potential Predictability of the spring bloom in the southern ocean sea ice zone: Data and analysis scripts [Dataset]. Zenodo. https://doi.org/10.5281/zenodo.8003803

Bushuk, M., Winton, M., Haumann, F. A., Delworth, T., Lu, F., Zhang, Y., et al. (2021). Seasonal prediction and predictability of regional Antarctic sea ice. *Journal of Climate*, *34*(15), 6207–6233. https://doi.org/10.1175/jcli-d-20-0965.1

Chassot, E., Bonhommeau, S., Dulvy, N. K., Mélin, F., Watson, R., Gascuel, D., & Pape, O. L. (2010). Global marine primary production constrains fisheries catches. *Ecology Letters*, *13*(4), 495–505. https://doi.org/10.1111/j.1461-0248.2010.01443.x

Chikamoto, M. O., Timmermann, A., Chikamoto, Y., Tokinaga, H., & Harada, N. (2015). Mechanisms and predictability of multiyear ecosystem variability in the North Pacific. *Global Biogeochemical Cycles*, *29*(11), 2001–2019. https://doi.org/10.1002/2015gb005096

Delworth, T. L., Broccoli, A. J., Rosati, A., Stouffer, R. J., Balaji, V., Beesley, J. A., et al. (2006). GFDL's CM2 global coupled climate models. Part I: Formulation and simulation characteristics. *Journal of Climate*, *19*(5), 643–674. https://doi.org/10.1175/jcli3629.1

Deppeler, S. L., & Davidson, A. T. (2017). Southern ocean phytoplankton in a changing climate. *Frontiers in Marine Science*, *4*, 40. https://doi.org/10.3389/fmars.2017.00040

Douglas, C. C., Briggs, N., Brown, P., MacGilchrist, G., & Naveira Garabato, A. (2023). Exploring the relationship between sea-ice and primary production in the Weddell gyre using satellite and argo-float data.
Dunne, J. P., John, J. G., Adcroft, A. J., Griffies, S. M., Hallberg, R. W., Shevliakova, E., et al. (2012). GFDL's ESM2 global coupled Climate–Carbon Earth system models. Part I: Physical formulation and baseline simulation characteristics. *Journal of Climate*, *25*(19), 6646–6665. https://doi.org/10.1175/jcli-d-11-00560.1
Dunne, J. P., John, J. G., Shevliakova, E., Stouffer, R. J., Krasting, J. P., Malyshev, S. L., et al. (2013). GFDL's ESM2 global coupled Climate–Carbon earth system models. Part II: Carbon system formulation and baseline simulation characteristics. *Journal of Climate*, *26*(7), 2247–2267. https://doi.org/10.1175/jcli-d-12-00150.1
Friedland, K. D., Stock, C., Drinkwater, K. F., Link, J. S., Leaf, R. T., Shank, B. V., et al. (2012). Pathways between primary production and fisheries yields of large marine ecosystems. *PLoS One*, *7*(1), e28945. https://doi.org/10.1371/journal.pone.0028945
Frölicher, T. L., Aschwanden, M. T., Gruber, N., Jaccard, S. L., Dunne, J. P., & Paynter, D. (2020). Contrasting upper and deep ocean oxygen response to protracted global warming. *Global Biogeochemical Cycles*, *34*(8). https://doi.org/10.1029/2020gb006601
Frölicher, T. L., Ramseyer, L., Raible, C. C., Rodgers, K. B., & Dunne, J. (2020). Potential predictability of marine ecosystem drivers. *Biogeosciences*, *17*(7), 2061–2083. https://doi.org/10.5194/bg-17-2061-2020
Griffies, S. M., Gnanadesikan, A., Dixon, K. W., Dunne, J. P., Gerdes, R., Harrison, M. J., et al. (2005). Formulation of an ocean model for global climate simulations. *Ocean Science*, *1*(1), 45–79. https://doi.org/10.5194/os-1-45-2005
Ham, Y.-G., Joo, Y.-S., & Park, J.-Y. (2021). Mechanism of skillful seasonal surface chlorophyll prediction over the southern Pacific using a global Earth system model. *Climate Dynamics*, *56*(1–2), 45–64. https://doi.org/10.1007/s00382-020-05403-2
Holland, M. M., Blanchard-Wrigglesworth, E., Kay, J., & Vavrus, S. (2013). Initial-value predictability of Antarctic sea ice in the community climate system model 3. *Geophysical Research Letters*, *40*(10), 2121–2124. https://doi.org/10.1002/grl.50410
Horvat, C., Bisson, K., Seabrook, S., Cristi, A., & Matthes, L. C. (2022). Evidence of phytoplankton blooms under Antarctic sea ice. *Frontiers in Marine Science*, *9*. https://doi.org/10.3389/fmars.2022.942799
Krumhardt, K. M., Lovenduski, N. S., Long, M. C., Luo, J. Y., Lindsay, K., Yeager, S., & Harrison, C. (2020). Potential predictability of net primary production in the ocean. *Global Biogeochemical Cycles*, *34*(6). https://doi.org/10.1029/2020gb006531
Le Grix, N., Zscheischler, J., Rodgers, K. B., Yamaguchi, R., & Frölicher, T. L. (2022). Hotspots and drivers of compound marine heatwaves and low net primary production extremes. *Biogeosciences*, *19*(24), 5807–5835. https://doi.org/10.5194/bg-19-5807-2022
Libera, S., Hobbs, W., Klocker, A., Meyer, A., & Matear, R. (2022). Ocean-sea ice processes and their role in multi-month predictability of Antarctic sea ice. *Geophysical Research Letters*, *49*(8), e2021GL097047. https://doi.org/10.1029/2021gl097047
Llort, J., Lévy, M., Sallée, J.-B., & Tagliabue, A. (2015). Onset, intensification, and decline of phytoplankton blooms in the Southern Ocean. *ICES Journal of Marine Science*, *72*(6), 1971–1984. https://doi.org/10.1093/icesjms/fsv053
Marchi, S., Fichefet, T., Goosse, H., Zunz, V., Tietsche, S., Day, J. J., & Hawkins, E. (2019). Reemergence of Antarctic sea ice predictability and its link to deep ocean mixing in global climate models. *Climate Dynamics*, *52*(5–6), 2775–2797. https://doi.org/10.1007/s00382-018-4292-2
Massonnet, F., Reid, P., Lieser, J. L., Bitz, C. M., Fyfe, J., & Hobbs, W. (2020). Assessment of summer 2019-2020 sea-ice forecasts for the southern ocean. Retrieved from https://fmassonn.github.io/sipnsouth.github.io/
Moore, J. K., & Abbott, M. R. (2000). Phytoplankton chlorophyll distributions and primary production in the southern ocean. *Journal of Geophysical Research*, *105*(C12), 28709–28722. https://doi.org/10.1029/1999JC000043
Moreau, S., Boyd, P. W., & Strutton, P. G. (2020). Remote assessment of the fate of phytoplankton in the Southern Ocean sea-ice zone. *Nature Communications*, *11*(1), 3108. https://doi.org/10.1038/s41467-020-16931-0
Morioka, Y., Doi, T., Iovino, D., Masina, S., & Behera, S. K. (2019). Role of sea-ice initialization in climate predictability over the Weddell Sea. *Scientific Reports*, *9*(1), 2457. https://doi.org/10.1038/s41598-019-39421-w
Park, J.-Y., Stock, C. A., Dunne, J. P., Yang, X., & Rosati, A. (2019). Seasonal to multiannual marine ecosystem prediction with a global Earth system model. *Science*, *365*(6450), 284–288. https://doi.org/10.1126/science.aav6634
Pohlmann, H., Botzet, M., Latif, M., Roesch, A., Wild, M., & Tschuck, P. (2004). Estimating the decadal predictability of a coupled AOGCM. *Journal of Climate*, *17*(22), 4463–4472. https://doi.org/10.1175/3209.1
Rohr, T., Long, M. C., Kavanaugh, M. T., Lindsay, K., & Doney, S. C. (2017). Variability in the mechanisms controlling southern ocean phytoplankton bloom phenology in an ocean model and satellite observations. *Global Biogeochemical Cycles*, *31*(5), 922–940. https://doi.org/10.1002/2016gb005615
Séférian, R., Bopp, L., Gehlen, M., Swingedouw, D., Mignot, J., Guilyardi, E., & Servonnat, J. (2014). Multiyear predictability of tropical marine productivity. *Proceedings of the National Academy of Sciences of the United States of America*, *111*(32), 11646–11651. https://doi.org/10.1073/pnas.1315855111
Stock, C. A., Dunne, J. P., & John, J. G. (2014). Drivers of trophic amplification of ocean productivity trends in a changing climate. *Biogeosciences*, *11*(24), 7125–7135. https://doi.org/10.5194/bg-11-7125-2014
Stock, C. A., John, J. G., Rykaczewski, R. R., Asch, R. G., Cheung, W. W. L., Dunne, J. P., et al. (2017). Reconciling fisheries catch and ocean productivity. *Proceedings of the National Academy of Sciences of the United States of America*, *114*(8), E1441–E1449. https://doi.org/10.1073/pnas.1610238114
Taboada, F. G., Barton, A. D., Stock, C. A., Dunne, J., & John, J. G. (2019). Seasonal to interannual predictability of oceanic net primary production inferred from satellite observations. *Progress in Oceanography*, *170*, 28–39. https://doi.org/10.1016/j.pocean.2018.10.010
Tagliabue, A., Kwiatkowski, L., Bopp, L., Butenschön, M., Cheung, W., Lengaigne, M., & Vialard, J. (2021). Persistent uncertainties in ocean net primary production climate change projections at regional scales raise challenges for assessing impacts on ecosystem services. *Frontiers in Climate*, *3*, 738224. https://doi.org/10.3389/fclim.2021.738224
Taylor, M. H., Losch, M., & Bracher, A. (2013). On the drivers of phytoplankton blooms in the Antarctic marginal ice zone: A modeling approach. *Journal of Geophysical Research: Oceans*, *118*(1), 63–75. https://doi.org/10.1029/2012jc008418
Uchida, T., Balwada, D., Abernathey, R., Prend, C. J., Boss, E., & Gille, S. T. (2019). Southern ocean phytoplankton blooms observed by biogeochemical floats. *Journal of Geophysical Research: Oceans*, *124*(11), 7328–7343. https://doi.org/10.1029/2019jc015355
Winton, M. (1999). A reformulated three-layer sea ice model. *Journal of Atmospheric and Oceanic Technology*, *17*(4), 525–531. https://doi.org/10.1175/1520-0426(2000)017<0525:artlsi>2.0.co;2

References From the Supporting Information

Burger, F., Terhaar, J., & Frölicher, T. (2022). Compound marine heatwaves and ocean acidity extremes. *Nature Communications*, *13*(1), 4722. https://doi.org/10.1038/s41467-022-32120-7